
PVNet: A LRCN Architecture for Spatio-Temporal Photovoltaic Power Forecasting from Numerical Weather Prediction

000
001
002
003
004
005
006
007
008
009
010
011
012
013
014
015
016
017
018
019
020
021
022
023
024
025
026
027
028
029
030
031
032
033
034
035
036
037
038
039
040
041
042
043
044
045
046
047
048
049
050
051
052
053
054
Anonymous Authors¹

Abstract

Photovoltaic (PV) power generation has emerged as one of the lead renewable energy sources. Yet, its production is characterized by high uncertainty, being dependent on weather conditions like solar irradiance and temperature. Predicting PV production, even in the 24 hour forecast, remains a challenge and leads energy providers to keep idle - often carbon emitting - plants. In this paper we introduce a Long-Term Recurrent Convolutional Network using Numerical Weather Predictions (NWP) to predict, in turn, PV production in the 24 hour and 48 hour forecast horizons. This network architecture fully leverages both temporal and spatial weather data, sampled over the whole geographical area of interest. We train our model on a NWP dataset from the National Oceanic and Atmospheric Administration (NOAA) to predict spatially aggregated PV production in Germany. We compare its performance to the persistence model and to state-of-the-art methods.

1. Introduction

As of early 2019, 184 out of 197 Parties have ratified the Paris Agreement, which was negotiated at the 21st Conference of the Parties (COP21) to reduce the risks and effects of climate change. These signatures show a world-wide awareness of global warming issues and a commitment on planning initiatives that mitigate greenhouse gas emissions. Countries are taking actions in order to better integrate renewable clean energies into their grids.

Solar photovoltaic (PV) production is one of the most popular renewable energy sources. According to the International Agency of Energy (IAE)¹, cumulative solar PV capacity

reached almost 398 GW in 2017, representing around 2% of global power output. Furthermore, solar PV is expected to lead renewable electricity capacity growth, increasing to over 1000 GW by 2023.

Integrating solar PV production into the energy grids requires an accurate and reliable forecast of the PV power, in order to guarantee the optimal management of energy demand and supply. Yet, accurate PV power forecasting remains a challenge as the PV output depends on fluctuating weather conditions, like solar irradiance or other meteorological factors (Li et al., 2016a).

1.1. Related Works

Many studies have tackled the challenge of PV power forecast. They rely on statistical time-series methods, physical methods, or ensemble methods which combine different models to enhance accuracy (Sobri et al., 2018). Widely used time-series models can be separated into two groups: linear and non-linear models. Linear time-series models used in PV forecast include the combination of auto-regressive models (AR) with moving average models (MA) into auto-regressive moving average models (ARMA) (Li et al., 2014; Kardakos et al., 2013). While linear models are usually more transparent towards their feature selection, non-linear models often show better prediction accuracy when enough data are available. Among non-linear time-series models, Artificial Neural Networks (ANN) have become increasingly popular for PV forecast (Ding et al., 2011; Kardakos et al., 2013; Dolara et al., 2015) and among them Recurrent Neural Networks (Malvoni et al., 2013) and Long-Short Term Memory Networks (Abdel-Nasser & Mahmoud, 2017; Gensler et al., 2017). We note that ANN models can be interpreted as a non-linear version of AR, also called NAR, while Recurrent Neural Networks can be seen as a type of non-linear ARMA, also called NARMA.

The most successful methods among the ones mentioned above are models adding Numerical Weather Prediction (NWP) like predictions of solar irradiance or temperature into the time-series approach. They may also include analytical physical models outputs, like atmospheric models and several types of Clear Sky Models (Inman et al., 2013). NWP can be obtained from the European Centre

¹Anonymous Institution, Anonymous City, Anonymous Region, Anonymous Country. Correspondence to: Anonymous Author <anon.email@domain.com>.

Preliminary work. Under review by the International Conference on Machine Learning (ICML). Do not distribute.

¹<https://www.iea.org/topics/renewables/solar/>

for Medium-Range Weather Forecasts (ECMWF)² and the National Oceanic and Atmospheric Administration (NOAA)³. Clear Sky Models, and additional physical models, are provided by open-source libraries (Holmgren et al., 2018). Time-series models including these additional inputs are referred to as ARMA model with exogenous inputs (ARMAX) for the linear versions (Kardakos et al., 2013) or NAR with exogenous inputs (NARX) (Di Piazza et al., 2016) as well as Artificial Neural Networks with multiples inputs (Malvoni et al., 2013; Dolara et al., 2015; Hossain et al., 2018; Oneto et al., 2018).

Adding NWP and physical model inputs to time-series models show better forecast prediction, yet limited computational resources as well as dataset sizes often prohibit studies to integrate an exhaustive list of these variables, especially in non-linear models. Instead, the impact of the variables is assessed by independent experiments (Kardakos et al., 2013) or by fitting regression models like multiregression analyses (Malvoni et al., 2013) or multivariate adaptive regression splines (Li et al., 2016a). Eventually, a subset of the variables may be selected for prediction. These variables selection analyses are conducted at specific locations, at four PV plants in Greece (Kardakos et al., 2013), one PV plant in Southern Italy (Malvoni et al., 2013) and in Macau (Li et al., 2016b), while the variables impact on the prediction is likely to be location-dependent.

In this paper, we present a method that takes into account the spatial distribution of the input variables, in order to simultaneously increase the model's inference capacity - an understanding of which inputs variables are important at which geographic locations - as well as the model's prediction accuracy. In the above studies, the spatial distribution of the NWP and physical models variables are not taken into account: models focus for example on solar irradiance or temperature only at the specific location of the target plant. The time-series and neural network architectures often model the temporal structure of the variables, not their spatial structure and initiatives to incorporate spatial information are often restricted to sparse data at neighboring plants for example (Gutierrez-Corea et al., 2016; Agoua et al., 2018). Yet, weather variables and physical model outputs on the zone surrounding a target plant are additional data, especially valuable while fitting non-linear flexible models, that can be integrated into the input data for higher accuracy. To the best of our knowledge, there is no model that fully integrates both temporal and dense spatial numerical weather predictions and physical models outputs in PV forecasting.

Meanwhile, flexible non-linear predictions models taking into account the spatio-temporal structure of the data,

like Long-Term Recurrent Convolutional Network (LRCN) (Donahue et al., 2015), 2D LSTM or Convolutional LSTM architectures (ConvLSTM) (Shi et al., 2015), have been successfully applied to a variety of problems. LRCN models have been used in activity recognition, image captioning and visual question answering (Donahue et al., 2015). A 2D LSTM model has been applied to traffic forecasting (Zhao et al., 2017) while a ConvLSTM has shown promising results on a precipitation forecast that predicts rainfall intensity in a local region on a very short time horizon (Shi et al., 2015) (also known as nowcasting), a weather-related prediction problem that shares similarities with PV forecast.

1.2. Contributions and Outline

This paper presents PVNet, a PV forecasting model that introduces a LRCN architecture in order to integrates past PV power 1D time-series with dense spatio-temporal NWP and physical models' inputs. Our model extends the state-of-the-art 1D time-series models by learning spatial features with CNN modules, whose channels encode the NWP and physical models variables. We focus our analysis on the day-ahead PV forecast, whose accuracy is known to be highly dependent on NWP integration, and which is particularly interesting as energy market bids are placed one day in advance. Our experimental results show that our architecture manages to leverage this additional spatial data for prediction accuracy. We train a highly non-linear prediction model that reaches a high accuracy on our validation dataset. Furthermore, our model provides a location-dependent assessment of the impact of the different input variables, through an occlusion sensitivity analysis that shows a strong inference capability.

In Section 2, we describe the data representation used for the PV power output and the NWP and physical models variables. We then present our spatio-temporal LRCN model PVNet, with its CNN and LSTM modules. Section 5 describes our experimental studies and accuracy results, as well as the results of the occlusion sensitivity analysis that validates our spatio-temporal approach.

2. Data Representation

2.1. Photovoltaic Panel

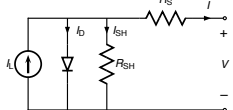
A photovoltaic solar panel, also called photovoltaic module, is a device that absorbs sunlight as a source of energy in order to generate electricity. We are interested in the power output produced by the module, which is a time series that depends on weather conditions, see Figure 2.

There are different ways to model the solar panel production from external factors, one of which is the equivalent electrical circuit of a solar cell is composed of a diode, a

²<https://www.ecmwf.int/en/forecasts/datasets/set-i>

³<https://www.emc.ncep.noaa.gov/GFS/doc.php>

110 resistor in series and in parallel as shown in see Figure 1⁴).



118 *Figure 1.* Equivalent Circuit of a Solar Cell.

119 The diode current is given by the Shockley diode equation:

$$122 \quad I_D = I_0(e^{\frac{V_j}{nV_T}} - 1) \quad (1)$$

124 With V_T :

$$125 \quad V_T = \frac{kT}{q} \quad (2)$$

128 With k the Boltzmann constant, T the absolute temperature
129 of the p-n junction, and q the elementary charge.

130 Thus the output power produced by the module obviously
131 depends on solar irradiance, but also on its temperature
132 (Fesharaki et al., 2011).

$$135 \quad P_{pv} = V_{pv} \times I_{pv} \quad (3)$$

$$139 \quad I_{pv} = I_l - I_0(e^{q(V_{pv} + I_{pv}R_s)/AKT} - 1) - \frac{V_{pv} + I_{pv}R_s}{R_{sh}} \quad (4)$$

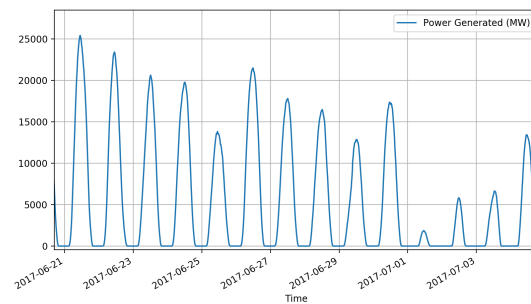
142 Furthermore, recent experimental research suggests that a
143 module's temperature is related to numerical weather data
144 such as the ambient temperature, the local irradiance and
145 wind speed. (Muzathik, 2014):

$$147 \quad T_m(^{\circ}\text{C}) = 0.94T + 0.02I - 1.5S + 0.35 \quad (5)$$

149 where T_m is the module's temperature, T is the *ambient*
150 temperature, I is the solar irradiance and S the wind speed.
151 However, this model essentially comes from an heuristic
152 and there are likely more weather data - and their non-linear
153 relationships - that could be taken into account to fully
154 characterize the module's temperature and hence, its power
155 output.

157 We just showed that the behavior of a photovoltaic panel is
158 both non linear because of its semi-conductor nature and
159 also dependant on the temperature of the panel. Temperature
160 which is itself dependant on external factors like external
161 temperature and windspeed which are available and forecast
162 through numerical services.

163 ⁴<https://commons.wikimedia.org>

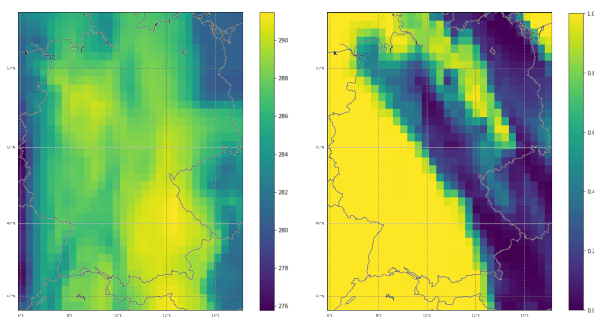


220 *Figure 2.* Aggregated power over a few days

2.2. Numerical Weather Predictions

We incorporate weather prediction data as well as their non-linear relationships in our model. Rather than just incorporating the irradiance and temperature at the specific location of the power plant(s), our model aims to leverage the full spatial scalar fields of the meteorological parameters over the whole area of interest. These forecasts can be obtained from global forecast systems, like the ECMWF HRES model (temporal resolution of 1 hour and spatial resolution of 0.1 degree)⁵ or the NOAA GFS⁶ (temporal resolution of 3 hours and spatial resolution of 0.5 degrees). Each of these models provide a set of weather-related variables.

Figure 3 shows examples of variables of interest, in this case over our country of interest Germany.



228 *Figure 3.* Temperature (in Kelvin) and Cloud Cover (unitless) maps
229 over Germany on May 1st, 2016

230 Figure 4 shows a collection of weather patches that typically
231 represents input data. Here one patch every three hours.

232 ⁵<https://www.ecmwf.int/en/forecasts/datasets/set-i>

233 ⁶<https://www.emc.ncep.noaa.gov/GFS/doc.php>

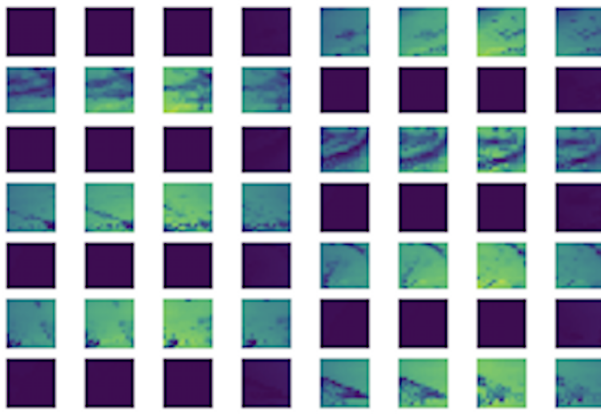


Figure 4. NOAA GFS Irradiance over Germany for 7 days - one patch every 3 hours - time goes from left to right. Lighter color values are higher irradiance. High level view show alternance of days and nights.

In order to predict PV power output in the day-ahead forecast, we use the numerical weather predictions of the above variables for this time horizon.

$$X_{NWP,t}(x,y) = \begin{pmatrix} NWP_1(x,y) \\ \vdots \\ NWP_K(x,y) \end{pmatrix} \quad (6)$$

where t is the time, measured in hours from the current time, (x,y) is the longitude-latitude coordinates of a point in the region of interest, and K is the number meteorological factors of interests.

We chose this set of weather features after investigating the intersection of various available data in the NWP forecast datasets and the current state of the art for the impact of the variables affecting the irradiance (here cloud cover and irradiance) and the performance of the solar panel (here outside temperature).

2.3. Incorporation of Standard Models Predictions

We also incorporate predictions of standard forecast models into our feature vector. We consider first the persistence model, a simple - yet popular - forecast model. The persistence model predicts that future PV output is likely to be similar as the current value at the same time of the day (Cornaro et al., 2015). We denote with the subscript PSS , the PV output predicted by a persistence model:

$$X_{PSS}(x,y,t) = P_{pv}(t - T_p) \quad (7)$$

where time T_p is measured in hours, and (x,y) the longitude-latitude coordinates. Here we take two specific values of persistence. One will be used for comparing the performance of the algorithm at T_{24} and the one we use as a

feature of our algorithm is at T_{48} . Indeed when used in the context of energy forecast, there is a 24 hours delay, as seen in figure 5.

A clear sky model estimates irradiance under the assumption that there are no clouds in the sky (Reno et al.) . This is a function of the altitude, location, and various atmospheric conditions. The irradiance predicted by the clear sky model is:

$$X_{CSM,t}(x,y) = CSM(t, x, y, \alpha(t, x, y)) \quad (8)$$

where t is the time, measured in hours from the current time, (x,y) is the longitude-latitude coordinates of a point in the region of interest and α is a set of external variables used for the Clear Sky Model. In our case we

Specifically, we form a feature at time t , X_t by aggregating the weather forecast variables with the predictions of the standard models:

$$X_t(x,y) = \begin{pmatrix} X_{NWP,t}(x,y) \\ X_{PSS,t} \\ X_{CSM,t}(x,y) \end{pmatrix} \in \mathbb{R}^{K+2} \quad (9)$$

where t is the time, measured in hours from the current time, (x,y) is the longitude-latitude coordinates of a point in the region of interest. thus, our feature vector incorporates both spatial weather forecasts as well as some predictions from existing models.

3. PVNet Model

The goal of PV power output forecasting is to use numerical weather predictions, to forecast the future PV output in a region, in our case: at the day ahead forecast at the scale of a country. We consider $t = 0$ the time at which we make the prediction, and thus $t_{\text{forecast}} = 24h$ is the forecast time. Precisely, we consider a sliding window of size T , and:

$$(X_{t_1}, \dots, X_{t_T}) \quad (10)$$

where X_t is the feature maps at time t , as defined in Equation 6 and $t_T = t_{\text{forecast}}$. Our goal is to predict:

$$\widehat{P}_{pv}(t_T),$$

an estimate of the PV production at the forecast horizon. Our training set is thus a set of $((X_{t_0+t_1}, \dots, X_{t_0+t_T}), P_{pv}(t_0 + t_T))_{t_0}$ for different values of t_0 .

Our model presents a long term recurrent convolutional network which combines a convolutional network (CNN) and a bi-directional long short term memory (LSTM) (Schuster & Paliwal, 1997) network, as shown in Figure 6. In practice,

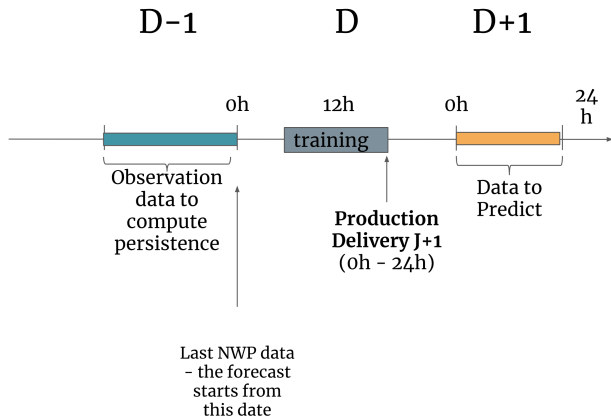


Figure 5. Timeline of day ahead prediction

we use a time window of $T = 8$ values, spread at 3 hours time interval, so as to represent a window that is a full day of data history.

3.1. The CNN Module

The model applies a convolutional neural network to each T images X_t of shape (width, height) and $K + 2$ number of channels. This results into a feature vector of dimension (T, d):

$$(x_{t_1}, \dots, x_{t_T}) = (g(X_{t_1}), \dots, g(X_{t_T})) \quad (11)$$

where each x_t is now a feature vector of dimension d . We use one single CNN architecture, and a single set of weights, to transform the feature X_t , independently of the time t . Therefore, this feature transformation step can be described by a single function g .

The aim of the CNN module is to encode the spatial data into a new feature vector of lower dimension as running the LSTM directly on the whole images would be too computationally expensive. Rather than hand-crafting spatially aggregated features, we let the CNN learn spatial features that are the most relevant for the following LSTM-based PV power predictions..

3.2. The LSTM Module

Each of the feature tensor is then fed into an LSTM (Hochreiter & Schmidhuber, 1997) network, to incorporate the time-series information. A LSTM network is a special case of Recurrent Neural Network (RNN), which introduces a memory cell c_t , that serves as an accumulator of state information. The cell c_t can be accessed, written and cleared by self-parameterized controlling gates. If the input gate i_t

is activated, the information of each new input, that is our feature vector x_t , is accumulated to the cell. If the forget gate f_t is activated, the previous cell status c_{t-1} can be forgotten. The output gate o_t controls if the cell output c_t will be propagated to the final state h_t . The model can be summarized with the following equations:

$$\begin{aligned} f_t &= \sigma_g(W_f x_t + U_f h_{t-1} + b_f) \\ i_t &= \sigma_g(W_i x_t + U_i h_{t-1} + b_i) \\ o_t &= \sigma_g(W_o x_t + U_o h_{t-1} + b_o) \\ c_t &= f_t \circ c_{t-1} + i_t \circ \sigma_c(W_c x_t + U_c h_{t-1} + b_c) \\ h_t &= o_t \circ \sigma_h(c_t) \end{aligned} \quad (12)$$

One of the limitations of the LSTM is that any hidden layer associated with a timestep t only has access to past data. Bidirectional RNNs (Schuster & Paliwal, 1997) have shown to be more efficient in natural language processing tasks (Arisoy et al., 2015). The following equations show how the RNN take into account past and future data:

$$\begin{aligned} \vec{h}_t &= f(\vec{W} x_t + \vec{V} \vec{h}_{t-1} + \vec{b}) \\ \overleftarrow{h}_t &= f(\overleftarrow{W} x_t + \overleftarrow{V} \overleftarrow{h}_{t-1} + \overleftarrow{b}) \\ \hat{y}_t &= g(U g_t + c) = g(U[\vec{h}_t; \overleftarrow{h}_t] + c) \end{aligned} \quad (13)$$

The intent of the BiLSTM module is to design features, at each time t that take into account the temporal structure of the input signal.

3.3. Full Model

The convolutional network extracts spatial features (in our case spatial weather related features) and then forwards them to the LSTM. We then have a fully connected layer taking all the LSTM hidden outputs and producing a single scalar value that is the estimated value of aggregated PV output prediction for the whole country.

We highlight that this model differs from the ConvLSTM model from (Shi et al., 2015), in the sense that the ConvLSTM model integrates convolutional structures directly in the LSTM cells.

Both CNN and LSTM modules are trained simultaneously, to minimize the mean squared error loss function:

$$MSE = \frac{1}{N} \sum_{t=t_0}^{t_N-1} \left(\widehat{P_{pv}}(t + t_T) - P_{pv}(t + t_T) \right)^2, \quad (14)$$

summed over window's initial time values t_0 .

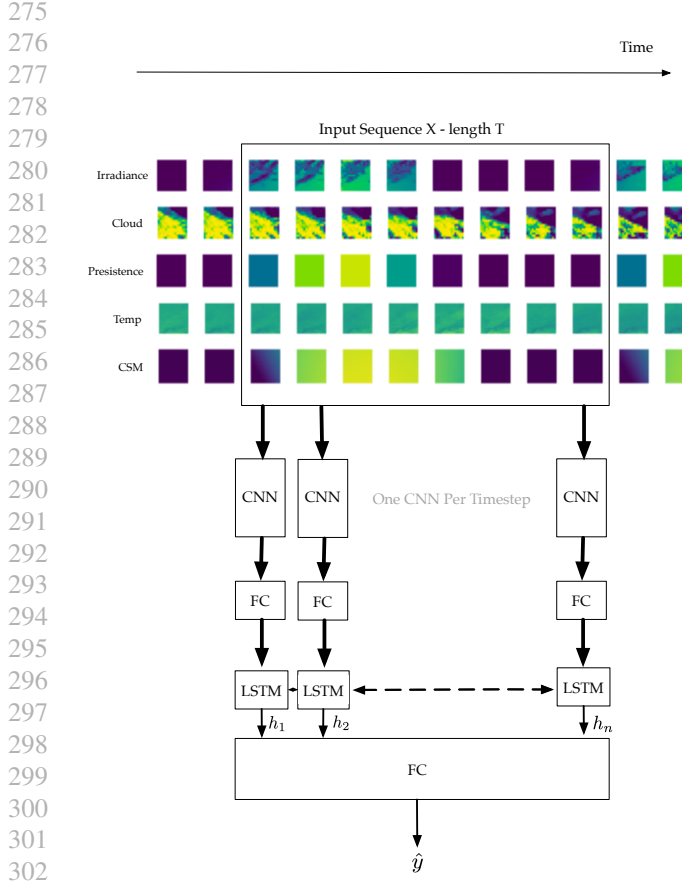


Figure 6. PVNet Architecture Details

3.4. Implementation Details

We implement PVNet using the Tensorflow (Abadi et al.) framework. Our convolutional networks are built alternating 2D convolution layers, PReLU activations (He et al.), dropout and max pooling.

There is also a 20% dropout after each convolutional layer. We added a fully connected layer between the CNN layers and the LSTM, with a 30% dropout in between.

In this implementation we use the hard sigmoid for the recurrent activation and the hyperbolic tangent for the activation itself.

4. Dataset

We consider an aggregated production of PV power across Germany. We gather past data from 2014 to 2018, sampled at a time resolution of 15 minutes.

We use numerical weather prediction data from the National Oceanic and Atmospheric Administration, more specifically the Global Forecasting System (GFS). This data is freely

Table 1. CNN Layers Details

LAYER	PARAMETERS	ACTIVATION
CONV2D	3x3x64	PReLU
CONV2D	3x3x64	PReLU
MAXPOOL	2x2	N/A
CONV2D	3x3x128	PReLU
CONV2D	3x3x128	PReLU
MAXPOOL	N/A	
CONV2D	3x3x256	PReLU
CONV2D	3x3x256	PReLU
MAXPOOL	2x2	
FLATTEN	N/A	N/A
FC	512	N/A

available, has a spatial resolution of 0.5 degrees of latitude and longitude and a time resolution of 3 hours. The time resolution of the PV power is downsampled at 3h, to match the time resolution of the NWP. We consider $K = 3$ meteorological variables: Downward short wave radiation flux (DSWRF), Cloud Cover (EACC) and Temperature (TMP). We incorporate data from the persistence model and the Clear Sky Model.

4.1. Time Alignment

Time alignment is extremely important for the training to work properly. When first looking at the GFS data one has to be careful about time shifts. The persistence data included in the model is not the one used to evaluate the performance of the model. Indeed in a production setting one only has access to the data from the day before. This means that we can only use persistence data from 48 hours before the point to estimate, whereas the actual persistence metrics is done 24 hours before.

4.2. Training and Validation Split

We split the training and validation dataset as follows: the first 3 years are used for training and the last year is used for validation. This approach guarantees that our validation score is not affected by seasonal patterns. Indeed, the duration of the day being very different between the summer and the winter solstice, performance measures could be affected without this specific care.

5. Experiments and Results

Our experiments are run on a computer with a single NVIDIA Titan X GPU. The training time of the network is 5 hours. We train our model using the Adam optimizer (Kingma & Ba, 2014), with a learning rate of 0.0015 and a batch size of 32. We run our training for a total of 500 epochs, as shown in Figure 7.

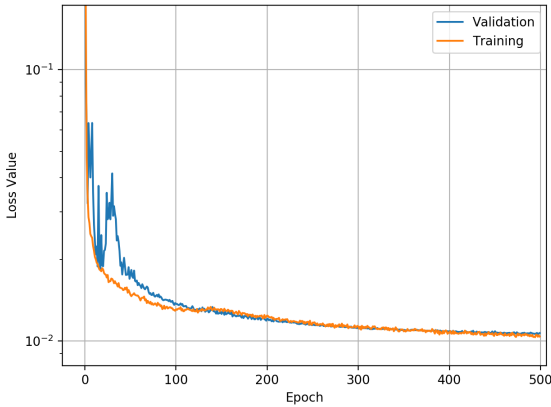


Figure 7. PVNet Training and Validation Losses for n=500 epochs.

5.1. Metrics and Results

We use two metrics to evaluate the quality of PVNet: the root mean squared error (RMSE) and mean absolute error (MAE) of the prediction. We compute these metrics only when the measured predicted power is higher than 0 ($P_{PV}(t) > 0$). We do not take nights into accounts because these values tend to increase the performance since the estimator of the PV night is trivially $\hat{P}_{PV}(t) = 0$. The normalized RMSE and MAE (nRMSE and nMAE) are normalized with the country-wide PV capacity, which is 41.2 GW in our case.

Tables 1 and 2 present our results for PVNet compared to the persistence model and the current state of the art for day ahead country wide PV prediction (Lorenz et al., 2011). (Lorenz et al., 2011) used data from 2009-2010 and a different formulation of the nRMSE. The authors of (Lorenz et al., 2011) indeed normalized the production on a per plant basis while we normalize it at the scale of the whole country. We re-implement their method in order to compute the metrics MAE, nMAE, RMSE and nRMSE for the same times as the ones used in our validation dataset.

We compute the persistence model RMSE by taking the value of the country-aggregated prediction 24 hours before the current value. We first observe a RMSE improvement of 17.31 percents compared to the persistence model, which is expected since the persistence model is fairly naive. We do also use the persistence data in our model as one of the inputs - even though the timing is quite different. We use 24 hours persistence for verification and 48 hours persistence as the PVNet input layer.

We also observe a 1.38% decrease in accuracy error in nRMSE and a 0.74% decrease in accuracy error in nMAE

Table 2. PVNet Experimental Performance

METHOD	NRMSE (%)	nMAE (%)
PERSISTENCE	22.04	15.28
LORENZ ET AL	6.11	4.37
PVNET	4.73	3.63

METHOD	RMSE (MW)	MAE (MW)
PERSISTENCE	8816	6297
LORENZ ET AL	2518	1798
PVNET	1949	1499

compared to the state of the art in country-wide day ahead aggregation (Lorenz et al., 2011). Non-linear spatio temporal features are being captured in much more details in PVNet, allowing a better overall performance.

5.2. Occlusion Sensitivity Analysis

One of the main interests of this model is to build a spatial representation of the impact of various variables (weather, clear sky model and persistence) on the aggregated PV production. One way to verify if this is the case is to perform a sensitivity analysis in order to evaluate the spatial impact of each variable.

This type of analysis has been shown to work well in the case of deep neural networks (Zeiler & Fergus, 2013).

We perform an occlusion sensitivity analysis by setting the values of a patch to a fixed value and recording the changes in value of the predicted power prediction. We perform this analysis for each channel and aggregated the values in a heatmap form. We then overlay this heatmap with the map of Germany and we obtain the results as shown in 8. The results show that our network sees the biggest impact with irradiance, followed by cloud cover, clear sky, persistence and finally temperature.

In order to compare the results of the sensitivity analysis we build a heatmap representing the distribution of PV power generated across Germany on May 1st, 2016. We aggregate the nominal capacity of the plants on a spatial grid of 0.25×0.25 degrees by summing all plant maximum power on this area. We overlay this heatmap with Germany country boundaries for more clarity (see figure 9). This clearly clearly that the south / east of Germany produces more power per squared meter, which is consistent with the results of our occlusion map. Indeed most of the metrics in the sensitivity maps (figure 8) show higher incidence in the south west.

This sensitivity analysis also shows which input features have the biggest impact on the outputs. Indeed we that in

order or decreasing importance, the values are irradiance, followed by cloud cover, the clear sky channel and finally Persistence and Temperature. This analysis also gives us a good insight about PVNet - looking at these two figures we can conclude that applying PV net and a Sensitivity analysis can be used to learn an estimate of the surface density of PV power production for a given area.

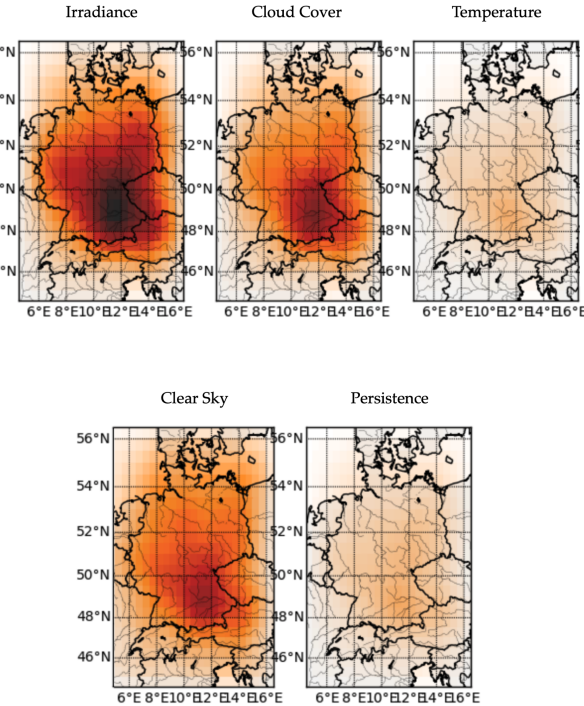


Figure 8. Occlusion Sensitivity Analysis for a 2x2 Patch. Black is highest sensitivity, white/light orange is lowest sensitivity.

6. Conclusion and Future Work

Global warming and the current energy crisis are both calling for the integration of renewable energies, including solar PV energy, into countries power grids. Yet, such an integration is still limited by our ability in making reliable PV power forecast. Accurate PV forecast remains challenging because of its correlation with highly fluctuating weather variables.

This paper introduced PVNet, a country-wide PV forecast model that fully integrates 1D time-series of past PV power with dense spatio-temporal exogenous inputs. Specifically, PVNet leverages a LRCN architecture that tackles spatio-temporal regression problems using numerical weather predictions and physical models as additional inputs. The

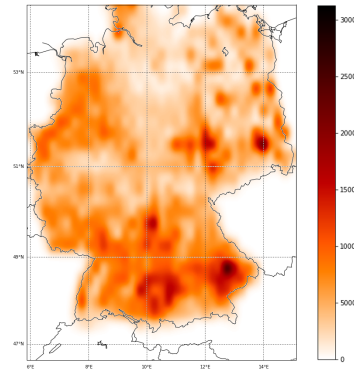


Figure 9. Distribution of PV power generated across Germany. The unit is power in Watts produced per area of 0.25×0.25 degrees of latitude and longitude.

model enjoys good performances in terms of prediction. Our results show a decrease in nRMSE of 1.38% compared to the state-of-the-art model for country-aggregated PV output prediction.

This LRCN model also demonstrates inference capability. NWP variables and physical models inputs have intricate and location-dependent correlations with PV power output. We showed that the CNN modules of the LRCN model are able to learn the geographic impact of different meteorological factors on the PV power prediction. Our occlusion sensitivity analysis validates our dense spatial approach and also allows us to better understand the dominant features as a function of location. It provides an interesting visualization tool for energy providers in order to estimate the effect of several weather variables of their PV power output. We also show that combining PVNet and a Sensitivity analysis can be used to learn an estimate of the surface density of PV power production for a given area.

Future work will first involve refinements of the current model, introducing for example interpolation of NWP inputs in order to avoid temporal down-sampling and data loss. Then, we will build on the LRCN architecture by incorporating new spatial information, like satellite imagery or fish-eye data imagery. A reliable PV forecast thus relies on models that fully leverage the available geographical data. With this work, we aim to open the doors to more spatio-temporal methods in PV output forecasting. The objective of such models is to enable a secure and economic integration of PV power into smart energy grids of countries over the world. This leads, in turn, to an increase of the proportion of renewable clean energies in the world's energy consumption.

References

- 440 Abadi, M., Agarwal, A., Barham, P., Brevdo, E., Chen, Z.,
 441 Citro, C., Corrado, G. S., Davis, A., Dean, J., Devin, M.,
 442 Ghemawat, S., Goodfellow, I., Harp, A., Irving, G., Is-
 443 ard, M., Jia, Y., Jozefowicz, R., Kaiser, L., Kudlur, M.,
 444 Levenberg, J., Mané, D., Monga, R., Moore, S., Mur-
 445 ray, D., Olah, C., Schuster, M., Shlens, J., Steiner, B.,
 446 Sutskever, I., Talwar, K., Tucker, P., Vanhoucke, V., Va-
 447 sudevan, V., Viégas, F., Vinyals, O., Warden, P., Watt-
 448 enberg, M., Wicke, M., Yu, Y., Zheng, X., and Research,
 449 G. TensorFlow: Large-Scale Machine Learning on Het-
 450 erogeneous Distributed Systems. Technical report. URL
 451 www.tensorflow.org.
 452
- 453 Abdel-Nasser, M. and Mahmoud, K. Accurate photovoltaic
 454 power forecasting models using deep LSTM-RNN. *Neu-
 455 ral Computing and Applications*, pp. 1–14, 2017. ISSN
 456 09410643. doi: 10.1007/s00521-017-3225-z.
 457
- 458 Agoua, X. G., Girard, R., and Kariniotakis, G. Probabilistic
 459 Model for Spatio-Temporal Photovoltaic Power Forecast-
 460 ing. *IEEE Transactions on Sustainable Energy*, 2018.
 461 ISSN 19493029. doi: 10.1109/TSTE.2018.2847558.
 462
- 463 Arisoy, E., Sethy, A., Ramabhadran, B., and Chen, S.
 464 Bidirectional recurrent neural network language mod-
 465 els for automatic speech recognition. In *2015 IEEE In-
 466 ternational Conference on Acoustics, Speech and Sig-
 467 nal Processing (ICASSP)*, pp. 5421–5425. IEEE, 4 2015.
 468 ISBN 978-1-4673-6997-8. doi: 10.1109/ICASSP.2015.
 469 7179007. URL [http://ieeexplore.ieee.org/
 470 document/7179007/](http://ieeexplore.ieee.org/document/7179007/).
 471
- 472 Cornaro, C., Pierro, M., and Bucci, F. Master optimiza-
 473 tion process based on neural networks ensemble for 24-h
 474 solar irradiance forecast. *Solar Energy*, 111:297–312,
 475 2015. ISSN 0038092X. doi: 10.1016/j.solener.2014.
 476 10.036. URL [http://dx.doi.org/10.1016/j.
 477 solener.2014.10.036](http://dx.doi.org/10.1016/j.solener.2014.10.036).
- 478 Di Piazza, A., Di Piazza, M. C., and Vitale, G. So-
 479 lar and wind forecasting by NARX neural networks.
 480 *Renewable Energy and Environmental Sustainability*,
 481 1:39, 2016. ISSN 2493-9439. doi: 10.1051/
 482 rees/2016047. URL [http://www.rees-journal.
 483 org/10.1051/rees/2016047](http://www.rees-journal.org/10.1051/rees/2016047).
- 484 Ding, M., Wang, L., and Bi, R. An ANN-based Approach
 485 for Forecasting the Power Output of Photovoltaic System.
 486 2011. doi: 10.1016/j.proenv.2011.12.196. URL [www.
 487 elsevier.com/locate/procedia](http://www.elsevier.com/locate/procedia).
- 488 Dolara, A., Grimaccia, F., Leva, S., Mussetta, M., and
 489 Ogliari, E. A physical hybrid artificial neural network
 490 for short term forecasting of PV plant power output. *En-*
 491 *ergies*, 8(2):1138–1153, 2015. ISSN 19961073. doi:
 492 10.3390/en8021138.
 493
- 494 Donahue, J., Hendricks, L. A., Guadarrama, S., Rohrbach,
 495 M., Venugopalan, S., Darrell, T., and Saenko, K. Long-
 496 term recurrent convolutional networks for visual recog-
 497 nition and description. In *Proceedings of the IEEE Com-
 498 puter Society Conference on Computer Vision and Pat-
 499 tern Recognition*, 2015. ISBN 9781467369640. doi:
 500 10.1109/CVPR.2015.7298878.
- 501 Fesharaki, V. J., Dehghani, M., Fesharaki, J. J., and
 502 Tavasoli, H. The Effect of Temperature on Photo voltaic Cell Efficiency. Technical report, 2011. URL http://research.iaun.ac.ir/pd/jjfesharakiol/pdf/PaperC_4124.pdf.
- 503 Gensler, A., Henze, J., Sick, B., and Raabe, N. Deep
 504 Learning for solar power forecasting - An approach us-
 505 ing AutoEncoder and LSTM Neural Networks. *2016
 506 IEEE International Conference on Systems, Man, and
 507 Cybernetics, SMC 2016 - Conference Proceedings*, pp.
 508 2858–2865, 2017. ISSN 1879-0852. doi: 10.1109/SMC.
 509 2016.7844673.
- 510 Gutierrez-Corea, F. V., Manso-Callejo, M. A., Moreno-
 511 Regidor, M. P., and Manrique-Sancho, M. T. Forecasting
 512 short-term solar irradiance based on artificial neural net-
 513 works and data from neighboring meteorological stations.
Solar Energy, 134:119–131, 2016. ISSN 0038092X. doi:
 514 10.1016/j.solener.2016.04.020. URL <http://dx.doi.org/10.1016/j.solener.2016.04.020>.
- 515 He, K., Zhang, X., Ren, S., and Sun, J. Delving Deep
 516 into Rectifiers: Surpassing Human-Level Performance on
 517 ImageNet Classification. Technical report. URL <https://arxiv.org/pdf/1502.01852.pdf>.
- 518 Hochreiter, S. and Schmidhuber, J. Long Short-Term Mem-
 519 ory. *Neural Computation*, 1997. ISSN 08997667. doi:
 520 10.1162/neco.1997.9.8.1735.
- 521 Holmgren, W. F., Hansen, C. W., and Mikofski, M. A.
 522 pvlib python: a python package for modeling solar en-
 523 ergy systems. 2018. doi: 10.21105/joss.00884. URL
<https://doi.org/10.21105/joss.00884>.
- 524 Hossain, M., Mekhilef, S., Danesh, M., Olatomiwa, L., and
 525 Shamshirband, S. Application of extreme learning
 526 machine for short term output power forecasting of
 527 three grid-connected PV systems. *Journal of Cleaner
 528 Production*, 167:395–405, 2018. ISSN 09596526. doi:
 529 10.1016/j.jclepro.2017.08.081. URL <http://dx.doi.org/10.1016/j.jclepro.2017.08.081>.
- 530 Inman, R. H., Pedro, H. T. C., and Coimbra, C. F. M. Solar
 531 forecasting methods for renewable energy integration.
 532 2013. doi: 10.1016/j.pecs.2013.06.002. URL <http://dx.doi.org/10.1016/j.pecs.2013.06.002>.

- 495 Kardakos, E. G., Alexiadis, M. C., Vagropoulos, S. I.,
 496 Simoglou, C. K., Biskas, P. N., and Bakirtzis, A. G.
 497 Application of time series and artificial neural network
 498 models in short-term forecasting of PV power genera-
 499 tion. *Proceedings of the Universities Power Engineering
 500 Conference*, pp. 1–6, 2013. ISSN 1944-9925. doi:
 501 10.1109/UPEC.2013.6714975.
- 502 Kingma, D. P. and Ba, J. Adam: A Method for Stochastic
 503 Optimization. 12 2014. URL <http://arxiv.org/abs/1412.6980>.
- 504 Li, Y., Su, Y., and Shu, L. An ARMAX model for
 505 forecasting the power output of a grid connected photo-
 506 voltaic system. 2014. doi: 10.1016/j.renene.2013.
 507 11.067. URL <http://dx.doi.org/10.1016/j.renene.2013.11.067>.
- 508 Li, Y., He, Y., Su, Y., and Shu, L. Forecasting the daily
 509 power output of a grid-connected photovoltaic system
 510 based on multivariate adaptive regression splines. *Applied
 511 Energy*, 180:392–401, 2016a. ISSN 03062619. doi: 10.
 512 1016/j.apenergy.2016.07.052. URL <http://dx.doi.org/10.1016/j.apenergy.2016.07.052>.
- 513 Li, Z., Mahboubur Rahman, S. M., Vega, R., and Dong,
 514 B. A hierarchical approach using machine learning
 515 methods in solar photovoltaic energy production fore-
 516 casting. *Energies*, 9(1), 2016b. ISSN 19961073. doi:
 517 10.3390/en9010055.
- 518 Lorenz, E., Heinemann, D., and Christian, K. Local and
 519 regional photovoltaic power prediction for large scale
 520 grid integration: Assessment of a new algorithm for snow
 521 detection. *International Journal of ChemTech Research*,
 522 9(11):261–270, 2011. ISSN 09744290. doi: 10.1002/pip.
 523
- 524 Malvoni, M., De Giorgi, M. G., and Congedo, P. M.
 525 Photovoltaic power forecasting using statistical methods:
 526 impact of weather data. *IET Science, Measurement
 527 & Technology*, 8(3):90–97, 2013. ISSN 1751-
 528 8822. doi: 10.1049/iet-smt.2013.0135. URL <http://digital-library.theiet.org/content/journals/10.1049/iet-smt.2013.0135>.
- 529 Muzathik, A. M. Photovoltaic Modules Operating Tempera-
 530 ture Estimation Using a Simple Correlation. *International
 531 Journal of Energy engineering*, 4:151–158, 2014. ISSN
 532 1470-2045.
- 533 Oneto, L., Laureri, F., Robba, M., Delfino, F., and An-
 534 guita, D. Data-driven photovoltaic power production
 535 nowcasting and forecasting for polygeneration micro-
 536 grids. *IEEE Systems Journal*, 12(3):2842–2853, 2018.
 537 ISSN 19379234. doi: 10.1109/JSYST.2017.2688359.
- 538 Reno, M. J., Hansen, C. W., and Stein, J. S. SAN-
 539 DIA REPORT Global Horizontal Irradiance Clear
 540 Sky Models: Implementation and Analysis. Technical
 541 report. URL <http://www.ntis.gov/help/ordermethods.asp?loc=7-4-0#online>.
- 542 Schuster, M. and Paliwal, K. K. Bidirec-
 543 tional Recurrent Neural Networks. Technical
 544 Report 11, 1997. URL <https://pdfs.semanticscholar.org/4b80/89bc9b49f84de43acc2eb8900035f7d492b2.pdf>.
- 545 Shi, X., Chen, Z., Wang, H., Yeung, D.-Y., Wong, W.-
 546 k., and Woo, W.-c. Convolutional LSTM Network: A
 547 Machine Learning Approach for Precipitation Nowcast-
 548 ing. pp. 1–12, 2015. ISSN 10495258. doi: 10.1074/
 549 jbc.M200827200. URL <http://arxiv.org/abs/1506.04214>.
- 550 Sobri, S., Koohi-Kamali, S., and Rahim, N. A. Solar pho-
 551 toovoltaic generation forecasting methods: A review. *En-
 552 ergy Conversion and Management*, 156(May 2017):459–
 553 497, 2018. ISSN 01968904. doi: 10.1016/j.enconman.
 554 2017.11.019. URL <https://doi.org/10.1016/j.enconman.2017.11.019>.
- 555 Zeiler, M. D. and Fergus, R. Visualizing and Under-
 556 standing Convolutional Networks. 11 2013. URL <http://arxiv.org/abs/1311.2901>.
- 557 Zhao, Z., Chen, W., Wu, X., Chen, P. C. Y., and Liu,
 558 J. LSTM network: a deep learning approach for
 559 short-term traffic forecast. *IET Intelligent Trans-
 560 port Systems*, 11(2):68–75, 2017. ISSN 1751-
 561 956X. doi: 10.1049/iet-its.2016.0208. URL <http://digital-library.theiet.org/content/journals/10.1049/iet-its.2016.0208>.